

## Dealloying of Platinum-Aluminum Thin Films: Dynamics of Pattern Formation

Henning Galinski,\* Thomas Ryll, Lukas Schlagenhauf, Felix Rechberger, Sun Ying, and Ludwig J. Gauckler  
*Nonmetallic Inorganic Materials, ETH Zurich, Zurich, Switzerland*

Flavio C. F. Mornaghini, Yasmina Ries, and Ralph Spolenak  
*Laboratory for Nanometallurgy, ETH Zurich, Zurich, Switzerland*

Max Döbeli

*Ion Beam Physics, ETH Zurich, Zurich, Switzerland*

(Received 3 May 2011; revised manuscript received 27 September 2011; published 21 November 2011)

The application of focused ion beam (FIB) nanotomography and Rutherford backscattering spectroscopy (RBS) to dealloyed platinum-aluminum thin films allows for an in-depth analysis of the dominating physical mechanisms of nanoporosity formation during the dealloying process. The porosity formation due to the dissolution of the less noble aluminum in the alloy is treated as result of a reaction-diffusion system. The RBS and FIB analysis yields that the porosity evolution has to be regarded as superposition of two independent processes, a linearly propagating diffusion front with a uniform speed and a slower dissolution process in regions which have already been passed by the diffusion front. The experimentally observed front evolution is captured by the Fisher-Kolmogorov-Petrovskii-Piskounov (FKPP). The slower dissolution is represented by a zero-order rate law which causes a gradual porosity in the thin film.

DOI: 10.1103/PhysRevLett.107.225503

PACS numbers: 81.16.Rf, 81.07.-b, 81.16.Dn, 82.80.Yc

In 1927, Murray Raney dealloyed nickel-aluminum alloys with concentrated sodium hydroxide in order to derive extremely porous and nanostructured nickel catalysts [1]. This process has gained renewed attention in recent years for the formation of nanoporous metallic thin films [2–9]. The interest is not only motivated by industrial needs of miniaturized sensors and catalysts [5] but also by fundamental interests in the physical mechanisms that control the pattern or porosity formation [4,6]. However, reliable measurements of the dealloying dynamics are rare and mostly indirect. It is usually assumed that the dealloying of the less noble metal in the alloy can be treated in terms of a phase separation at the reaction interface via a mean field approach described by the nonlinear Cahn-Hilliard equation [2,4,6]. Dealloying is a reaction-diffusion process, where the less noble metal in a solid solution is dissolved at the solid-liquid interface to an acid or alkaline solution. But, there are no previous measurements in these fast reaction-diffusion systems providing evidence of a propagating diffusion front and a measurement of its speed.

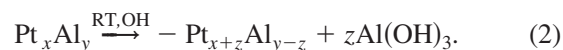
Therefore the main objective of this Letter is to reveal the presence of these system-specific characteristics during dealloying in a thin film geometry. A combined experimental and theoretical approach has been chosen that treats the observable macroscopical changes in the composition and morphology of the thin film in terms of a reaction-diffusion equation (RDE). For normal diffusion, this RDE reads

$$\frac{\partial}{\partial t} c(x, t) = R(c) + D \frac{\partial^2}{\partial x^2} c(x, t), \quad (1)$$

where  $c(x, t)$  is the local concentration,  $R(c)$  is a system-specific reaction term and  $D$  the diffusion coefficient

[10–12]. Because of the large aspect ratio of the thin film, the reaction and diffusion processes can be treated in one dimension. The Pt/Al system has been selected for its nearly complete miscibility between the two elements including the formation of various intermetallic phases. Pt/Al layers of 300 nm in thickness were deposited at room temperature by magnetron cosputtering ( $P_{\text{Pt}} = 37 \text{ W}$ ,  $P_{\text{Al}} = 252 \text{ W}$ ,  $p_{\text{Ar}} = 2.6 \times 10^{-3} \text{ mbar}$ ) onto amorphous  $\text{Si}_3\text{N}_4$  substrates that were precleaned using isopropanol and acetone.

In order to achieve a measurement scheme of sufficient significance, the substrates coated with the Pt/Al thin film were dealloyed in 4M NaOH at room temperature in a time domain between 1–10 s in steps of  $\Delta t = 1 \text{ s}$ . The reaction between the thin film and the basic solution can be established to



The morphological and compositional analysis of the samples was studied via FIB and RBS. Single and multiple cross-sections of the dealloyed Pt/Al systems were cut, polished and imaged using a Zeiss NVISION 40 FIB etching system. The stacks of multiple cross sections were aligned recursively by Stackreg [13] and reconstructed using AVS Express (Advanced Visual Systems, Inc.). The voxel size of the resulting tomographic images is  $2.17 \times 2.17 \times 6.5 \text{ nm}^3$ . The compositional analysis was performed by RBS experiments using a 2 MeV  $^4\text{He}$  beam and a standard silicon surface barrier detector at  $165^\circ$ . The background was subtracted using a common fitting procedure [14]. The elemental composition

and diffusion profiles were obtained using the RUMP program [15]. For the investigated films RBS provides a quantitative one-dimensional depth profile of the composition with a depth resolution of 10 to 20 nm [16].

In Fig. 1(a), the spatial arrangement of the Pt/Al-phase as obtained by the FIB nanotomography reconstruction after 10 s of dealloying is shown. The dealloying results in a fine branchlike pattern with a median branch thickness of 17(3) nm and a mean pore intercept length of 10(3) nm. The formed pattern is nonuniform and characterized by a strong directive gradient porosity as function of the film thickness  $h$ . This gradient porosity, as shown in Fig. 1(b), is substantiated by calculating the porosity by grey-level thresholding [17] from multiple cross sections of the dealloyed Pt/Al film. The porosity increases with increasing film thickness  $h$  from 20 area.% to 80 area.%. In the vicinity of the film-ambient interface a zone of roughly 25 nm thickness is observed where the porosity evolution changes its functional shape significantly. The zone denoted by \* in Fig. 1(b) is assumed to originate from the prolonged exposure to the alkaline solution. This caused the nearly complete dissolution of the Al in the film which

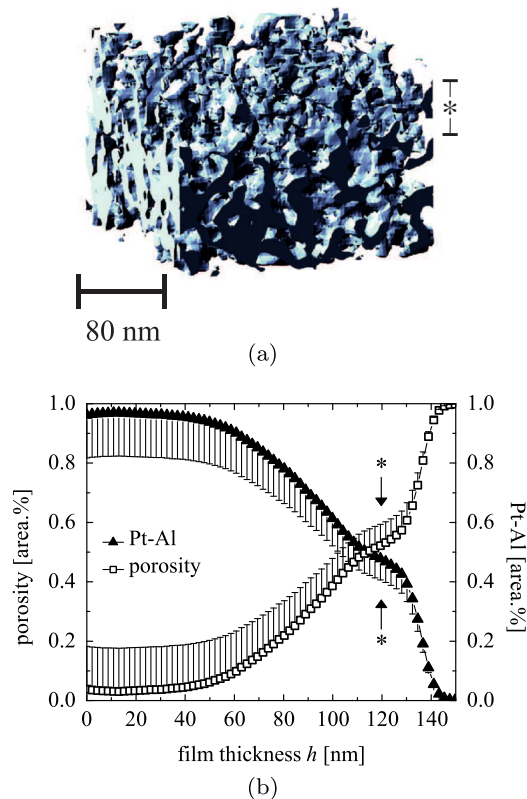


FIG. 1 (color online). (a) Three-dimensional (3D) reconstruction of a dealloyed 120 nm-thick  $\text{Pt}_{72}\text{Al}_{28}$  film on  $\text{Si}_3\text{N}_4$  obtained via FIB nanotomography. (b) Mean porosity as function of the film thickness  $h$ . Regions denoted by \* indicate deviations due to the dissolution of Pt causing film shrinkage and a steeper porosity gradient.

consequently led to the dissolution of the Pt and thus to a shrinkage of the film.

In order to further evaluate the dynamics of pattern formation, time-resolved RBS spectra have been measured and analyzed using the RUMP software. From the simulated spectra, critical time-dependent parameters like the spatial composition  $\eta$ , the thickness of each layer  $h$ , the mean diffusion coefficient  $D$  and additional loss of Al in the dealloyed layer have been determined. The thickness  $h_i$  of each layer is related to the yield of backscattered particles  $Q(E)$  (peak height) by

$$Q(E) = I_0 \Omega_0 \frac{d\sigma(E)}{d\Omega} h_i, \quad (3)$$

whereby  $I_0$  is the number of incident particles,  $\Omega_0$  the detector solid angle and  $\frac{d\sigma(E)}{d\Omega}$  the differential scattering cross section [16]. The resulting RBS spectra and their corresponding simulation using  $\eta$ ,  $h$ ,  $X_i$  as fitting parameters are shown in Fig. 2(a).

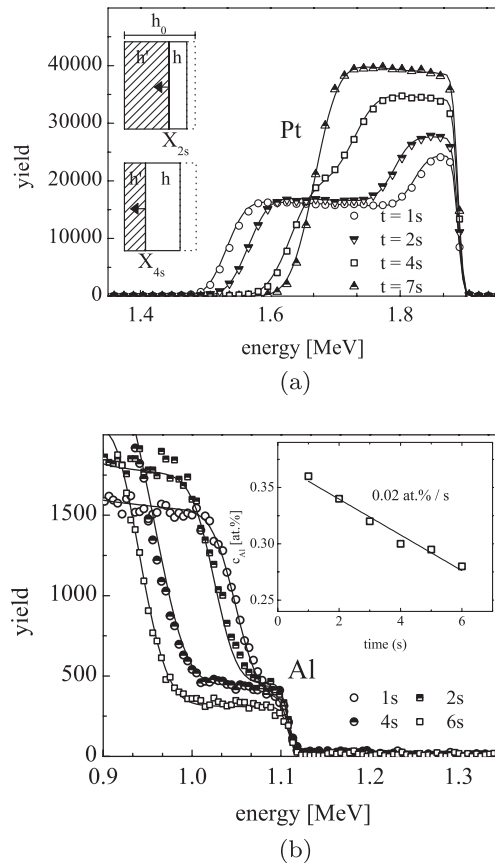


FIG. 2. Plots of the subtracted 2 MeV  $^4\text{He}$  RBS spectra of the time-resolved dealloying of Pt/Al thin films (dots) and simulated spectra (solid lines) using RUMP. (a) Pt peak. A schematic illustration of the dealloying process including the position of the diffusion front  $X_i$ , the dealloyed layer thickness  $h$  and the thickness  $h'$  of the remaining dense thin film is given in the inset. (b) Al peak. The inset depicts the measured Al loss in the already dealloyed layer.

The RBS measurements in Fig. 2(a) verify the dissolution of Al as function of time, which manifests in the steplike profile of the envelope of the two Pt peaks. The right shoulder of the envelope corresponds to the Al-deficient dealloyed Pt layer with thickness  $h$ , whereas the left shoulder corresponds to the remaining  $\text{Pt}_{24}\text{Al}_{76}$  thin film with thickness  $h'$ . In addition, a shrinkage of the Pt/Al film in the order of  $-25(3)$  nm/s is indicated by a decrease of the envelope width as function of time. The position of the dissolution front  $X_t$  is calculated with respect to the initial film thickness  $h_0$  and thus considers the layer shrinkage [dotted outline in the inset of Fig. 2(a)] in the dealloyed layer. In Fig. 2(b), there is a clear trend of decreasing Al concentration (decreasing peak height) as function of time in the already dealloyed layer. Further analysis revealed, that the additional Al loss in the already dealloyed layer is  $\eta = 0.02$  at.%/s and scales linearly with time, see inset of Fig. 2(b). These results are in accordance to the microstructural findings in Fig. 1 and present clear evidence that the formed pattern is not solely defined by the reactive processes close to the propagation diffusion front but also by diffusion processes in the bulk of the alkaline solution.

The shrinkage-corrected position  $X_t$  of the traveling diffusion front scales linearly with time  $t$  and the corresponding velocity of this monotonic travelling front is  $v_f = \partial_t X_t = 42(3)$  nm/s; see Fig. 3(a). All relevant data have been summarized in Table I.

The experimental observation of an initially flat liquid-film interface that evolves with time to a propagating diffusion front with a constant front velocity  $v_f$  are specific characteristics of the Fisher-Kolmogorov-Petrovskii-Piskounov (FKPP) equation obeying a traveling wave solution with  $u(x, t) = \psi(x - v_f t)$  [18]. The FKPP equation reads as follows

$$\frac{\partial}{\partial t} u(x, t) = D \frac{\partial^2}{\partial x^2} u(x, t) + \mu u(x, t)(1 - u(x, t)), \quad (4)$$

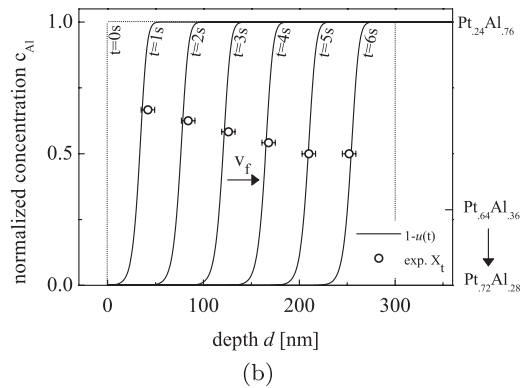
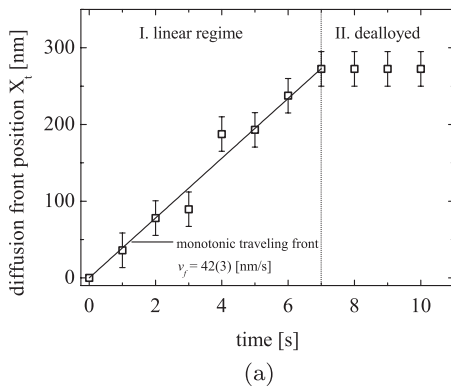


FIG. 3. (a) Propagation front velocity  $v_f = \partial_t X_t$  derived from the shrinkage-corrected front positions  $X_t$  obtained by RUMP simulations. (b) Comparison of the diffusion fronts obtained by numerical solution of 4 in the case of  $\mu = 11.0(8)$  at.%/s and  $D = 4.2(13) \times 10^{-17}$  m<sup>2</sup>/s with front positions  $X_t$  calculated using  $v_f$ .

where  $\mu$  represents the reaction rate of the system. The FKPP equation is a well known and widely applied non-linear reaction-diffusion equation [10,19] and is traditionally applied to model the spread of genes in population genetics [11]. Using structural stability arguments [20], it can be shown that the front velocity  $v_f$  is solely defined by the reaction rate  $\mu$  and the diffusion coefficient  $D$  and reads

$$v_f = 2\sqrt{\mu D}. \quad (5)$$

Using the experimentally determined values for  $v_f$  and  $D$ , the reaction rate of the dealloying system is determined to  $\mu = 11.0(8)$  at.%/s. Thereafter, Eq. (4) has been solved numerically using MATHEMATICA with a Heaviside step function  $H(x)$  as initial condition  $u(0, t) = 1 - H(x)$ . To match the experimental conditions though, the corresponding solutions is established to be  $c(x, t) = 1 - u(x, t)$ . In Fig. 3,  $c(x, t)$  with  $\mu = 11.0(8)$  at.%/s and  $D = 4.2(13) \times 10^{-17}$  m<sup>2</sup>/s have been plotted in comparison to the experimentally determined front positions  $X_t$ . The chosen reactive diffusion equation fits nicely to the measured diffusion front positions  $X_t$ , although it does not feature the measured additional Al loss in the early stage of dealloying. By choosing  $c(x, t) = 1 - u(x, t)$  the reaction term of the RD system becomes  $R(c) = \mu c(x, t)(c(x, t) - 1)$ , this kind of reaction-diffusion systems describe branching random walk phenomena, like branching Brownian motion [21]. In the present case, the branching event can be interpreted as the dissolution of Al out of the Pt/Al alloy whose space is then occupied by the alkaline solution. Thereby the spatial occupation grows linearly with time [22], as also proven experimentally in Fig. 3.

In essence, it has been shown that the dynamics of dealloying can be treated as a reaction-diffusion system. Thereby the used FKPP equation reproduces the experimental characteristics in a satisfactory manner. The RD-system is fully characterized by the measured propagation

TABLE I. Measured initial and final alloy compositions  $\eta_0$  and  $\eta_{\text{end}}$ , diffusion front velocity  $v_f$ , film shrinkage  $\partial_t h$  and the mean diffusion coefficient  $D$ .

$\eta_0$ [at. %]	$\eta_{\text{end}}$ [at. %]	$v_f$ [nm/s]	$\partial_t h$ [nm/s]	$D$ [m <sup>2</sup> /s]
Pt <sub>24</sub> Al <sub>76</sub>	Pt <sub>72</sub> Al <sub>28</sub>	42(3)	-25(3)	$4.2(13) \times 10^{-17}$

front velocity  $v_f = 42(3)$  nm/s and the diffusion coefficient  $D = 4.2(13) \times 10^{-17}$  m<sup>2</sup>/s.

In addition, experimental evidence indicates that the pattern formation related to the dealloying process can be regarded as a superposition of the reaction-diffusion system confined to the solid/liquid interface and an additional dissolution process with  $\eta = 0.02$  at. %/s in the bulk of the alkaline solution. Therefore the dealloying dynamics can be separated in two independent processes represented by a system of two decoupled partial differential equations

$$\frac{\partial}{\partial t_1} c(x_1, t_1) = D \frac{\partial^2}{\partial x_1^2} c(x_1, t_1) + \mu c(x_1, t_1) [c(x_1, t_1) - 1] \quad (6)$$

$$\frac{\partial}{\partial t_2} \tilde{c}(x_2, t_2) = -\eta \cdot H(X_t - x_2), \quad (7)$$

where  $c$  is the Al concentration involved in the first process of decomposition, i.e., the linearly propagating diffusion front, described by Eq. (6) and  $\tilde{c}$  is the residual Al concentration, whose evolution is captured by Eq. (7). Hence, the FKPP equation forms together with a zero-order rate law the basis of the nonlinear reactive diffusion system taking a linearly propagating diffusion front and the secondary dissolution  $\eta$  of Al in regions that have already been passed by the diffusion front ( $x_2 < X_t$ ) into account. The latter process is much slower than the propagating diffusion front but it has a severe impact on the endform of the dealloyed pattern and the porosity distribution. The present results contrast the common theoretical assumption that the dealloying is confined to the interface of the diffusion front [2,6]. It is noteworthy that all input parameters  $D$ ,  $v_f$ ,  $\eta$  of Eq. (6) and (7) have been determined experimentally.

In an upcoming work, the dealloyed films are analyzed in matters of their catalytical properties and stability during an oxygen reduction reaction [23].

The authors gratefully acknowledge the financial supported by the Swiss Bundesamt für Energie (BfE), Swiss Electric Research (SER), the Competence Center of Energy and Mobility (CEM) and the Swiss National

Foundation (SNF). We would like to thank the EMEZ (Electron Microscopy Center, ETH Zurich) for their support. Henning Galinski would like to thank Anna Evans, Iwan Schenker, Philippe Gasser and Barbara Scherrer for fruitful and stimulating discussions.

\*henning.galinski@mat.ethz.ch

- [1] M. Raney, US Patent No. 1628190 1927.
- [2] J. Erlebacher, M. J. Aziz, A. Karma, N. Dimitrov, and K. Sieradzki, *Nature (London)* **410**, 450 (2001).
- [3] J. Erlebacher, in *Dekker Encyclopedia of Nanoscience and Nanotechnology*, edited by J. A. Schwarz, C. I. Contescu, K. Putyera (Marcel Dekker Inc., New York, 2004), p. 893.
- [4] J. Erlebacher, *J. Electrochem. Soc.* **151**, C614 (2004).
- [5] R. Yang, P. Strasser, and M. F. Toney, *J. Phys. Chem. C* **115**, 9074 (2011).
- [6] C. Eilks and C. Elliott, *J. Comput. Phys.* **227**, 9727 (2008).
- [7] A. J. Forty, *Nature (London)* **282**, 597 (1979).
- [8] M. C. Simmonds, H. Kheyrandish, J. S. Colligon, M. L. Hitchman, N. Cade, and J. Iredale, *Corrosion Science* **40**, 43 (1998).
- [9] J. C. Thorp, K. Sieradzki, L. Tang, P. A. Crozier, A. Misra, M. Nastasi, D. Mitlin, and S. T. Picraux, *Appl. Phys. Lett.* **88**, 033110 (2006).
- [10] R. D. Benguria and M. C. Depassier, *Phys. Rev. Lett.* **77**, 1171 (1996).
- [11] R. Fisher, *Ann. Eugenics* **7**, 355 (1937).
- [12] C. R. Doering, C. Mueller, and P. Smereka, *Physica (Amsterdam)* **325A**, 243 (2003).
- [13] P. Thévenaz, U. Ruttimann, and M. Unser, *IEEE Trans. Image Process.* **7**, 27 (1998).
- [14] M. Döbeli, *Nucl. Instrum. Methods Phys. Res., Sect. B* **249**, 800 (2006).
- [15] L. R. Doolittle, *Nucl. Instrum. Methods Phys. Res., Sect. B* **15**, 227 (1986).
- [16] M. A. N. Yongqiang Wang, *Handbook of Modern Ion Beam 5 Materials Analysis* (Materials Research, Warrendale, Pa., 2009).
- [17] A. Brink, *Pattern Recogn. Lett.* **9**, 335 (1989).
- [18] W. van Saarloos, *Phys. Rev. A* **39**, 6367 (1989).
- [19] A. Lemarchand, A. Lesne, and M. Mareschal, *Phys. Rev. E* **51**, 4457 (1995).
- [20] G. C. Paquette, L.-Y. Chen, N. Goldenfeld, and Y. Oono, *Phys. Rev. Lett.* **72**, 76 (1994).
- [21] E. Brunet and B. Derrida, *Europhys. Lett.* **87**, 60010 (2009).
- [22] H. P. McKean, *Commun. Pure Appl. Math.* **28**, 323 (1975).
- [23] T. Ryll, H. Galinski, L. Schlagenhauf, F. Rechberger, Y. Sun, L. J. Gauckler, F. C. F. Mornaghini, Y. Ries, R. Spolenak, and M. Doebeli, [arXiv:1108.5132](https://arxiv.org/abs/1108.5132).